Optimal design of wide-view-angle waveplate used for polarimetric diagnosis of lithography system

Honggang Gu [a], Hao Jiang [a], Chuanwei Zhang [a, b], Xiuguo Chen [a], and Shiyuan Liu [a, b, *]

[a] State Key Laboratory of Digital Manufacturing Equipment and Technology, Huazhong University of Science and Technology, Wuhan 430074, China

[b] Wuhan Eoptics Technology Co., Ltd., Wuhan 430075, China

ABSTRACT

The diagnosis and control of the polarization aberrations is one of the main concerns in a hyper numerical aperture (NA) lithography system. Waveplates are basic and indispensable optical components in the polarimetric diagnosis tools for the immersion lithography system. The retardance of a birefringent waveplate is highly sensitive to the incident angle of the light, which makes the conventional waveplate not suitable to be applied in the polarimetric diagnosis for the immersion lithography system with a hyper NA. In this paper, we propose a method for the optimal design of a wide-view-angle waveplate by combining two positive waveplates made from magnesium fluoride (MgF_2) and two negative waveplates made from sapphire using the simulated annealing algorithm. Theoretical derivations and numerical simulations are performed and the results demonstrate that the maximum variation in the retardance of the optimally designed wide-view-angle waveplate is less than ± 0.35° for a wide-view-angle range of ± 20°.

Keywords: wide-view-angle waveplate, immersion lithography, polarimetric diagnosis, optimal design, simulated annealing algorithm.

1. INTRODUCTION

Lithography is a key technology for the mass production of large scale integrated circuits. As the miniaturization of semiconductor devices accelerates, immersion lithography tools utilizing polarization illumination systems and hyper numerical aperture (NA) imaging systems have been developed to enhance the resolution [1-3]. However, the polarization effects associated with the polarization illumination and hyper-NA projection lens affect the imaging quality significantly, such as degradation in the contrast of fine images [4-6]. Therefore, it is highly desirable to diagnose and control the polarization aberrations in a hyper-NA immersion lithography system. The Mueller matrix ellipsometer (MME) and the Stokes polarimeter (SP) have been developed as powerful tools for the characterization of polarization properties of polarized light and samples [7, 8]. Since the polarization aberrations can be described by the Stokes-Mueller formulas [9], lithographers introduced the MME and SP to measure the polarization characteristics of the illumination and the projection lens, respectively [10-13].

Optical retarders are basic and indispensable optical elements in ellipsometry and polarimetry sytstems to modulate and analyze the polarization state of the polarized light by introducing a phase shift named as the retardance between the two orthogonal components of a polarized light. The waveplate made from birefringent materials is one of the most commonly used retarders due to its compact size and stable performances [8, 14]. A conventional waveplate is usually designed for collimated light at normal incidence, and the retardance varies greatly with the incident angle of light [15]. Since the light beam in a hyper-NA immersion lithography system illuminates the waveplate with wide-view angles, the retardance deviates greatly from its nominal value which make the conventional waveplate is not suitable to be used any more. It is therefore important to design wide-view-angle waveplates to meet the requirements in the applications of polarimetric diagnosis for a lithography system.

The reported methods for the design of wide-view-angle waveplates can be summarized as combining waveplates made from positive and negative birefringent materials to compensate the nonuniform deviation in retardance resulted by the

* Corresponding author: shyliu@hust.edu.cn; phone: +86 27 87559543; webpage: http://www2.hust.edu.cn/nom.

Optical Microlithography XXIX, edited by Andreas Erdmann and Jongwook Kye, Proc. of SPIE
Vol. 9780, 97801M · © 2016 SPIE · CCC code: 0277-786X/16/$18 · doi: 10.1117/12.2219139

illumination-cone ray angle. Y. Furutono and H. Nomura developed a wide-view-angle waveplate for the application in the polarization effect detection of a hyper NA immersion lithography system [16]. The wide-view-angle waveplate comprises two positive birefringent waveplates made from quartz compensated by two negative birefringent waveplates made from sapphire. J. Dong and Y. Li improved the design on the basis of Y. Furutono's work by performing an enumerative algorithm to obtain an optimal design for wide-view-angle waveplate [17]. K. Tan *et al*. proposed an approach to introduce a C-plate made from a stack of thin-film layers to compensate the A-plate made from hybrid liquid crystal (HyLC) to obtain a flat retardance response to the incident angle [18]. However, the quartz waveplate will exhibit strong optical activity at oblique incidence [19], and the HyLC waveplate can be used only in visible wavelength range, and the manufacturing process is complex. They did not explain how to select the initial thicknesses of the component waveplates to ensure the design process repeatable and reliable. In addition, the compromise between the resolution of the step size and the time cost of the enumerative algorithm prevents Dong *et al*. from finding a more optimal design.

Aiming at dealing with the above issues, this paper presents a method for the optimal design of a wide-view-angle waveplate by combining two positive waveplates made from magnesium fluoride (MgF_2) and two negative waveplates made from sapphire using the simulated annealing algorithm. We derive a simple and general theory for the retardance calculation of the birefringent crystal waveplate under arbitrary incident angle and azimuthal angle based on the theory of wave propagation. To ensure the design process repeatable and reliable, an approximate method to calculate the initial design parameters of the wide-view-angle waveplate is proposed. Further we apply the simulated annealing algorithm to obtain an optimal design of the wide-view-angle waveplate around the initial design parameters. Numerical results show that the optimal design of the wide-view-angle waveplate has a very flat retardance with the maximum variation less than ± 0.35° over a wide-view-angle range of ± 20°.

2. METHODS

2.1 Retardance formula of birefringent waveplates under oblique incidence

Waveplates made of birefringent crystals are the most commonly used optical retarders in ellipsometry and polarimetry systems. A single-waveplate is a slice of birefringent crystal usually cut with the optic axis lying on the plane of the plate. A conventional composite waveplate usually consists of multi single-waveplates and is designed and used for the condition of normal incidence with a nominal retardance between the two orthogonal components of a polarized light parallel and perpendicular to the direction of the optic axis. When the light propagates through the waveplate at the normal incidence, the retardance of the waveplate introduced by the birefringence and the optical path length in the crystal is given by

$$\delta = \frac{2\pi}{\lambda} \Delta n \cdot d, \tag{1}$$

where $\Delta n = n_e - n_o$ is the birefringence of the crystal, n_e and n_o are the refractive indices for the extraordinary ray (e-ray) and the ordinary ray (o-ray) of the polarized light, d is the effective optical path length of the waveplate, and λ is the vacuum wavelength.

The retardance of a birefringent waveplate is sensitive to the incident angle of the light since both the optical path length and the extraordinary refractive index vary with the direction of light propagation. Strict calculation of the retardance for arbitrary incident angle can be achieved by using the ray-tracing formulas or Maxwell's equations and boundary conditions [20-22]. However, these methods can be very complex. Here, we propose a simple formula to calculate the retardance of a waveplate under arbitrary incident angle and azimuthal angle based the theory of wave propagation.

Figure 1 schematically shows the wave propagation in a composite waveplate at oblique incidence in a Cartesian coordinate system assuming the optic axes of the single-waveplates lie parallel to x-axis or y-axis. The single-waveplates are numbered as 1, 2, …, I in the order of light propagation, and d_i represents the thickness of the i-th single-waveplate. The light **SO** enters the waveplate with an incident angle ε and an azimuth angle θ with respect to x-axis, and **S'O** is the projection of **SO** on x-y plane. $\mathbf{C}_i\mathbf{A}_i$ and $\mathbf{D}_i\mathbf{B}_i$ are the wave normals for e-ray and o-ray of the polarized light in the i-th single-waveplate, and γ_{ei} and γ_{oi} are their refraction angles, respectively. According to Snell's law, we can obtain

$$\sin\varepsilon = n_i \sin\gamma_{ei} = n_{oi} \sin\gamma_{oi}, \tag{2}$$

where n_i is the effective refractive index for the e-ray in the i-th single-waveplate with respect to the incident angle ε and azimuthal angle θ of the incident light. At oblique incidence, the refractive index for the o-ray will remain constant, while the refractive index of the e-ray will change with the incident angle ε and azimuthal angle θ of the incident light and can be calculated as [23, 24]

$$n_i = n_{ei}\left[1+\left(\frac{1}{n_{ei}^{\,2}}-\frac{1}{n_{oi}^{\,2}}\right)\cos^2\varphi_i\right]^{\frac{1}{2}}, \tag{3}$$

where n_{ei} and n_{oi} are the refractive indices for the e-ray and o-ray in the i-th single-waveplate at normal incidence, and φ_i is the intersection angle between the light beam and the optic axis of the i-th single-waveplate. Assuming the optic axes of the single-waveplates lie parallel to x-axis or y-axis, Eq. (3) can be rewritten as

$$n_i = n_{ei}\left[1+\left(\frac{1}{n_{ei}^{\,2}}-\frac{1}{n_{oi}^{\,2}}\right)\sin^2\varepsilon\cos^2\theta\right]^{\frac{1}{2}}, \tag{4a}$$

or

$$n_i = n_{ei}\left[1+\left(\frac{1}{n_{ei}^{\,2}}-\frac{1}{n_{oi}^{\,2}}\right)\sin^2\varepsilon\sin^2\theta\right]^{\frac{1}{2}}. \tag{4b}$$

Equation (4a) and (4b) are utilized when the optic axis of the i-th single-waveplate is parallel to x-axis and y-axis, respectively.

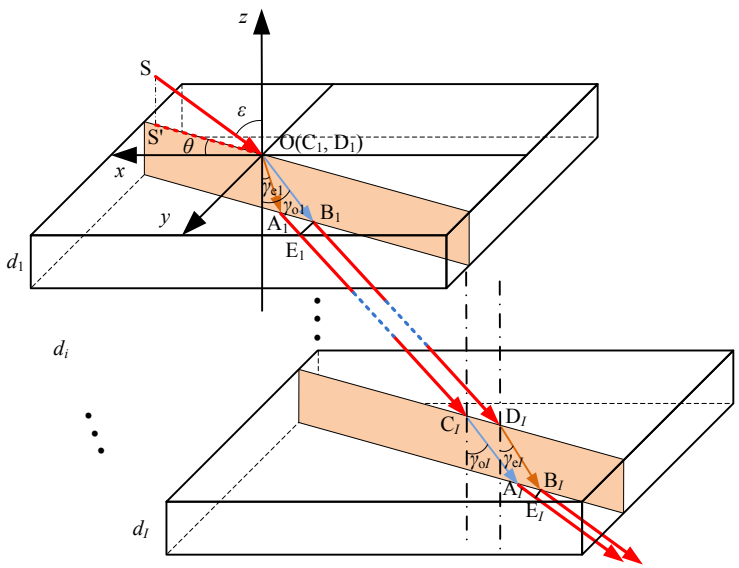

Figure 1. Schematic of the wave propagation in a waveplate under the incident angle ε and azimuth θ of the incident light.

According to the theory of wave propagation, the retardance of the waveplate is given by

$$\delta = \sum_{i=1}^{I}\frac{2\pi}{\lambda}L_i, \tag{5}$$

where λ is the vacuum wavelength, and L_i is the optical path difference between the e-ray and o-ray of the polarized light in the i-th single-waveplate, which is given by

$$L_i = \left|\mathrm{C_i A}_i\right| n'_{ei} + \left|\mathrm{D}_i \mathrm{B}_i\right| n_{oi} + \left|\mathrm{A}_i \mathrm{E}_i\right| = d_i \left[\frac{n'_{ei}}{\cos\gamma_{ei}} - \frac{n_{oi}}{\cos\gamma_{oi}} + \left(\tan\gamma_{ei} - \tan\gamma_{oi}\right)\sin\varepsilon \right], \tag{6}$$

where d_i is the thickness of the i-th single-waveplate.

2.2 Construction of a wide-view-angle waveplate

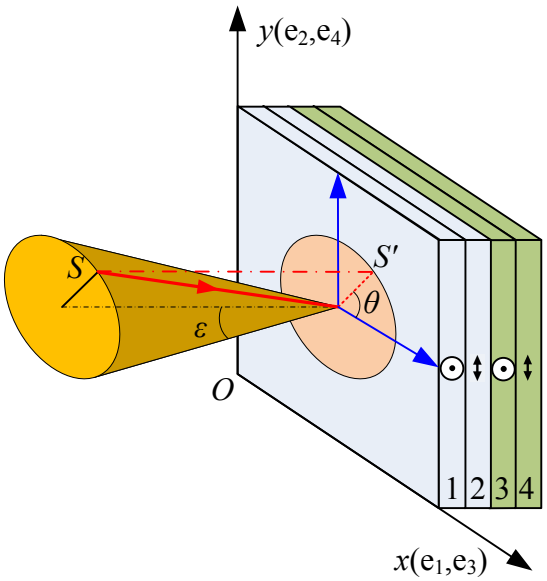

Figure 2. Schematic of the wide-view-angle waveplate consists of two positive waveplates made from MgF_2 and two negative waveplates made from sapphire, ε and θ are the incident angle and the azimuthal angle of the incident light. The optic axes of the 1-st and 3-rd single-waveplates (i.e., e_1 and e_3) are parallel to x-axis, while the optic axes of the 2-nd and 4-th single-waveplates (i.e., e_2 and e_4) are parallel to y-axis.

As schematically shown in Fig. 2, the wide-view-angle waveplate proposed in this paper consists of two positive waveplates made from MgF_2 and two negative waveplates made from sapphire to compensate the nonuniform deviation in retardance resulted by the illumination-cone ray angle. Compared with quartz, MgF_2 and sapphire exhibit negligible optical activity. For normal incidence, the two MgF_2 waveplates compose a compound zero-order quarter-wave waveplate, and the two sapphire waveplates compose a compound zero-order 0-wave waveplate. Thus, according to Eq. (1), we have

$$d_1 - d_2 = \frac{1}{4} \cdot \frac{\lambda}{\Delta n_\mathrm{m}}, \tag{7a}$$

$$d_3 - d_4 = 0 \cdot \frac{\lambda}{\Delta n_\mathrm{s}}, \tag{7b}$$

where d_i (i = 1, 2, 3, 4) is the thickness of the i-th single-waveplate, $\Delta n_\mathrm{m} = n_\mathrm{em} - n_\mathrm{om}$ and $\Delta n_\mathrm{s} = n_\mathrm{es} - n_\mathrm{os}$ are the birefringences of MgF_2 and sapphire, and n_em (n_om) and n_es (n_os) are the refractive index for the e-ray (o-ray) of MgF_2 and that of sapphire, respectively.

According to Eq. (3), we define the partial derivative of the effective refractive index for the e-ray to the incident angle as following

$$n_i' = \frac{\partial n_i}{\partial \varphi_i} = n_{ei}\left(\frac{1}{n_{ei}^2} - \frac{1}{n_{oi}^2}\right)\left[1 + \left(\frac{1}{n_{ei}^2} - \frac{1}{n_{oi}^2}\right)\cos^2\varphi_i\right]^{-\frac{1}{2}} \sin\varphi_i \cos\varphi_i, \tag{8}$$

To make a wide-view-angle waveplate, the thicknesses of the MgF_2 and sapphire waveplates should approximately satisfies the following relation

$$\frac{d_m}{d_s} \approx -\frac{n_s'}{n_m'}, \tag{9}$$

where d_m and d_s represent the thicknesses of MgF_2 waveplate and sapphire waveplate, n'_s and n'_m are the partial derivatives of the effective refractive index for the e-ray of MgF_2 and sapphire to the incident angle, and can be calculated by Eq. (8).

2.3 Optimal design of the wide-view-angle waveplate

The optimal design of a wide-view-angle waveplate aims to minimize the maximum deviation in the retardance over the view-angle range. Thus, the criterion for the optimal design of a wide-view-angle waveplate can be described as

$$\mathbf{D}_o = \arg \min_{\mathbf{D}\in[\mathbf{D}_0-\Delta d,\mathbf{D}_0+\Delta d]}\left[\max_{\varepsilon\in[-\phi,\phi];\theta\in[0,360°]}\left|\delta(\mathbf{D},\varepsilon,\theta)-90°\right|\right], \tag{10}$$

where, $\mathbf{D} = [d_1, d_2, d_3, d_4]$ refer to the thicknesses of the single-waveplates in the wide-view-angle waveplate, $\mathbf{D}_o = [d_{1o}, d_{2o}, d_{3o}, d_{4o}]$ and $\mathbf{D}_0 = [d_{10}, d_{20}, d_{30}, d_{40}]$ refer to the optimal thicknesses and the initial thicknesses of the single-waveplates respectively, ϕ and Δd are the ranges of change for the thickness and the incident angle and they are setting parameters in the optimal process, and $\delta(\mathbf{D}, \varepsilon, \theta)$ is the retardance of the wide-view-angle waveplate under the incident angle ε and azimuthal angle θ and can be calculated by Eq. (5).

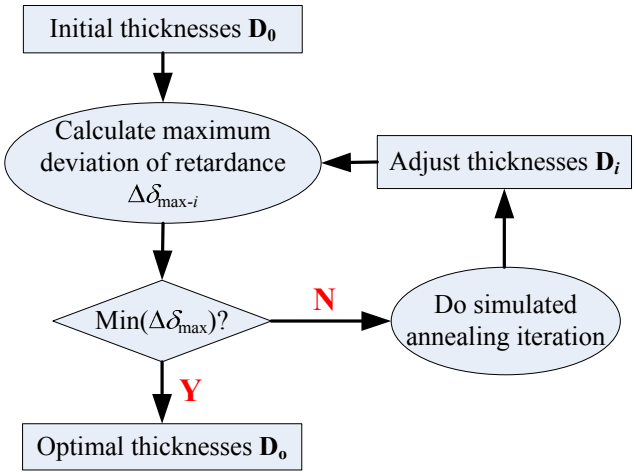

Figure 3. Flowchart of the optimal design of the wide-view-angle waveplate using simulated annealing algorithm.

In this paper, we use the simulated annealing algorithm to complete the optimal design process of the wide-view-angle waveplate. The simulated annealing algorithm is a generalized Monte Carlo algorithm and can help to obtain the optimal thicknesses of the single-waveplates efficiently [25]. The flowchart of the optimal process the wide-view-angle waveplate based on the simulated annealing algorithm is shown in Fig. 3. The initial thicknesses of the single-waveplates can be roughly calculated through Eq. (7)-(9).

3. NUMERICAL RESULTS

In this section, we present the numerical results of a wide-view-angle quarter-wave waveplate for the polarimetric diagnosis of a 193nm immersion lithography system with an NA of 1.35 as a concrete example to verify the proposed method. In this case, the waveplate is used over a wide-view-angle range of ± 20°. The refractive indices of MgF_2 and sapphire at the wavelength of 193nm are $(n_{em}, n_{om}) = (1.441, 1.428)$ and $(n_{es}, n_{os}) = (1.917, 1.929)$. According to the current level of polishing, we select the thickness of thinner one of the two MgF_2 single-waveplates as 100μm, i.e., $d_2 = 100\mu m$. Through Eq. (7)-(9), we can obtain the initial thicknesses of the four single-waveplates are $\mathbf{D}_0 = (d_{10}, d_{20}, d_{30}, d_{40}) = (103.71, 100, 199.91, 199.91)\mu m$. Further, we set the range of change for the thickness as $\Delta d = 10\mu m$, i.e., the ranges of the thicknesses of the single-waveplates are $[\mathbf{D}_0 - \Delta d, \mathbf{D}_0 + \Delta d] = [(93.71, 90, 189.91, 189.91)\mu m, (113.71, 110, 209.91, 209.91)\mu m]$.

Based on the above conditions, we can complete the optimal design of the wide-view-angle waveplate according to the procedure shown in Fig. 3 and Eq. (10). Figures 4-6 and Table 1 show the results of the optimally designed wide-view-angle waveplate for a 193nm immersion lithography system with an NA of 1.35.

TABLE 1. Thicknesses of the optimally designed wide-view-angle waveplate

Parameter	d_{1o}	d_{2o}	d_{3o}	d_{4o}
Thickness (μm)	104.55	101.59	204.85	204.04

Table 1 shows the optimal thicknesses of the single-waveplates in the wide-view-angle waveplate. It can be seen from Tab. 1 that the two MgF_2 single-waveplates no longer compose a compound zero-order quarter-wave waveplate and the two sapphire single-waveplates either no longer compose a compound zero-order 0-wave waveplate for the optimally designed wide-view-angle waveplate. The construction of these single-waveplates provides a rather flat retardance with the maximum deviation less than ± 0.35° from the nominal value over a wide-view-angle range of ± 20°, as shown in Fig. 4. To make a comparision, here we also present the retardance image of a conventional MgF_2 quarter-wave waveplate at the wavelength of 193nm as shown in Fig. 5. The thicknesses of the single-waveplates in the conventional MgF_2 waveplate are 103.71μm and 100μm. It can be observed from Fig. 5 that the maximum deviation in the retardance of the conventional MgF_2 waveplate from its nominal value is larger than 145°.

From Fig. 4 and Fig. 5, we can see that there are three special azimuthal angles for the retardances of the birefringent waveplate at oblique incidence, i.e., $45° + m\cdot 90°$, $0° + m\cdot 180°$, and $90° + m\cdot 190°$, where m is an integer. As shown in Fig. 6, the retardance remains unchanged with incident angle at the azimuth of 45°, while the retardance has the maximum deviation from its nominal value at the azimuth of 0° and 90°.

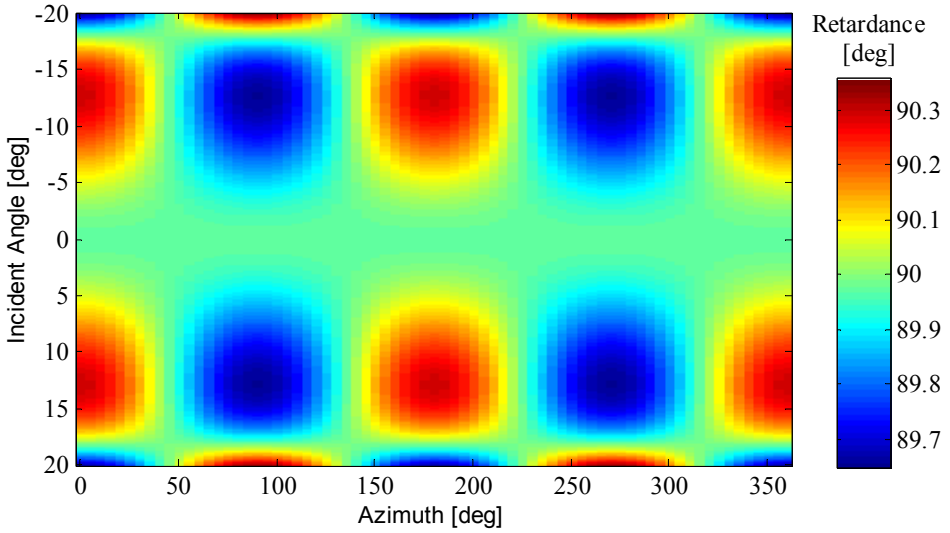

Figure 4 Retardance of the optimal wide-view-angle waveplate versus view-angle and azimuth angle at wavelength of 193nm.

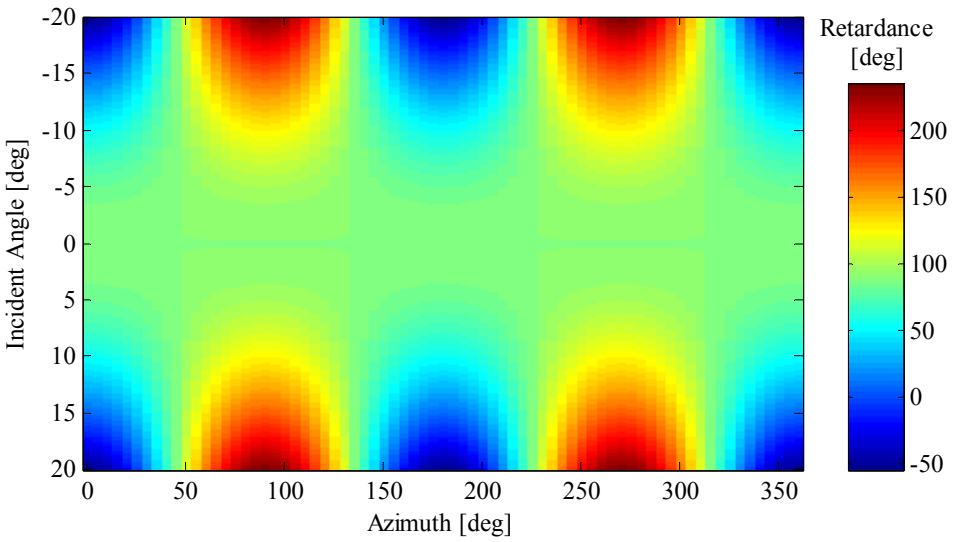

Figure 5 Retardance of the conventional MgF_2 quarter-wave waveplate versus view-angle and azimuth angle at wavelength of 193nm.

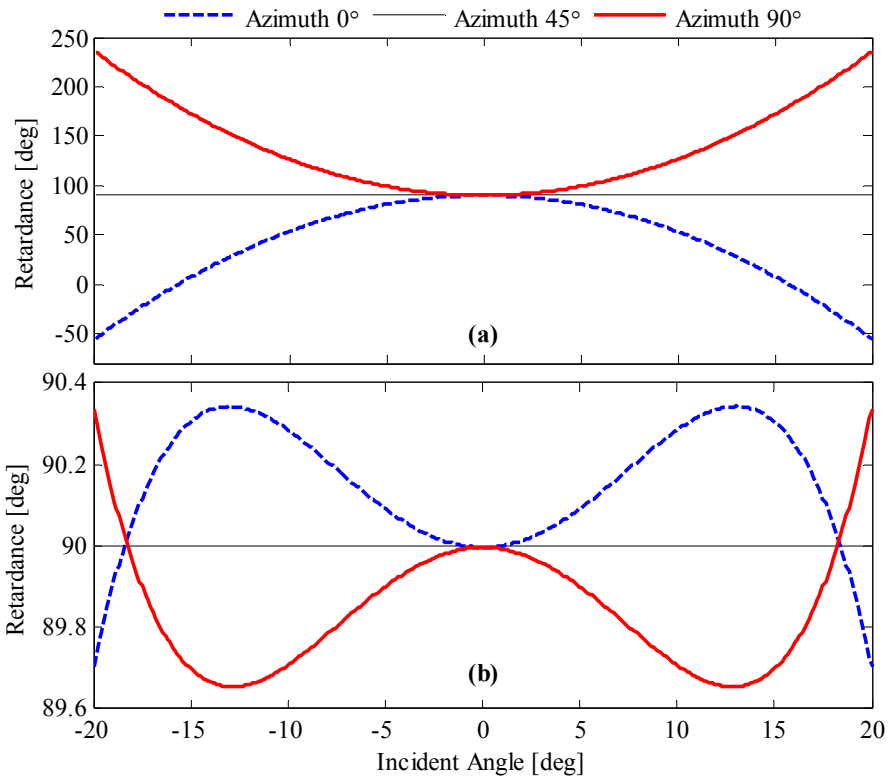

Fig. 6 Retardance versus view-angle at azimuthal angles of 0°, 45° and 90° at the wavelength of 193nm, (a) conventional MgF_2 waveplate; (b) optimal wide-view-angle waveplate.

4. CONCLUSIONS

In summary, we propose a method for the optimal design of a wide-view-angle waveplate for the polarimetric diagnosis of a lithography system by combining two positive waveplates made from magnesium fluoride (MgF_2) and two negative

waveplates made from sapphire using the simulated annealing algorithm. We derive a simple and general formula for the retardance calculation of the waveplate, and propose an approximate method to calculate the initial thicknesses of the wide-view-angle waveplate. Further we propose the optimal design process of the wide-view-angle waveplate using the simulated annealing algorithm. Numerical simulations have been performed and the results demonstrate that the maximum deviation in the retardance of the optimally designed wide-view-angle waveplate is less than ± 0.35° over a wide-view-angle range of ± 20°.

ACKNOWLEDGMENT

This work was funded by the National Natural Science Foundation of China (51475191, 51405172, 51575214, and 51525502); the Natural Science Foundation of Hubei Province of China (2015CFB278 and 2015CFA005); China Postdoctoral Science Foundation (2014M560607 and 2015T80791); and the Program for Changjiang Scholars and Innovative Research Team in University of China (IRT13017).

REFERENCES

[1] J. H. Bruning, "Optical lithography … 40 years and holding," *Proc. SPIE* **6520**, 652004 (2007).
[2] H. J. Mann and W. Ulrich, "Reflective high-NA projection lenses," *Proc. SPIE* **5962**, 596214 (2005).
[3] H. Nishinaga, N. Tokuda, S. Owa, S. Hirukawa, O. Tanitsu, T. Kudo, and H. Tanaka, "Development of polarized-light illuminator and its impact," *Proc. SPIE* **5754**, 669-680 (2005).
[4] D. Flagello, B. Geh, S. Hansen, and M. Totzeck, "Polarization effects associated with hyper-numerical-aperture (>1) lithography," *J. Microlithogr. Microfabr. Microsyst.* **4**(3), 031104 (2005).
[5] J. E. Webb, R. L. Maier, D. S. Goodman, and W. Conley, "Hyper-numerical aperture imaging challenges for 193 nm," *Proc. SPIE* **5754**, 69-79 (2005).
[6] J. Kye, G. R. McIntyre, Y. Norihiro, and H. J. Levinson, "Polarization aberration analysis in optical lithography systems," *Proc. SPIE* **6154**, 61540E (2006).
[7] S. Liu, X. Chen, and C. Zhang, "Development of a broadband Mueller matrix ellipsometer as a powerful tool for nanostructure metrology," *Thin Solid Films* **584**, 176-185 (2015).
[8] H. Gu, X. Chen, H. Jiang, C. Zhang, and S. Liu, "Optimal broadband Mueller matrix ellipsometer using multi-waveplates with flexibly oriented axes," *J. Opt.* **18**, 025702 (2016).
[9] G. R. McIntyre, J. Kye, H. J. Levinson, and A. R. Neureuther, "Polarization aberrations in hyper-numericalaperture projection printing: a comparison of various representations," *J. Microlithogr. Microfabr. Microsyst.* **5**(3), 033001 (2006).
[10] H. Nomura and Y. Furutono, "*In-situ* polarimetry of illumination for 193-nm lithography," *Proc. SPIE* **6924**, 69241T (2008).
[11] H. Nomura and I. Higashikawa, "In-situ Mueller matrix polarimetry of projection lenses for 193-nm lithography," *Proc. SPIE* **7640**, 76400Q (2010).
[12] H. Nomura, "Polarimetric diagnosis of 193-nm lithography equipment using a mask with newly developed polarization optical elements," *Thin Solid Films* **519**, 2688-2693 (2011).
[13] H. Nomura and Y. Furutono, "Polarimetry of illumination for 193nm immersion lithography," *Microelectronic Engineering* **85**, 1671-1675 (2008).
[14] H. G. Gu, S. Y. Liu, X. G. Chen, and C. W. Zhang, "Calibration of misalignment errors in composite waveplates using Mueller matrix ellipsometry," *Appl. Opt.* **54**(4), 684-693 (2015).
[15] P. D. Hale and G. W. Day, "Stability of birefringent linear retarders (waveplates)," *Appl. Opt.* **27**(24), 5146-5153 (1988).
[16] Y. Furutono and H. Nomura, "Wide-view-angle $\lambda/4$ plates for diagnosing 193-nm lithography tools," *Opt. Rev.* **16**(2), 188-191 (2009).
[17] J. Dong and Y. Li, "Analysis and optimization approaches for wide-viewing-angle k/4 plate in polarimetry for immersion lithography," *J. Vac. Sci. Technol. B* **31**(1), 011602 (2013).
[18] K. Tan, K. Hendrix, and P. Mckenzie, "Thin films provide wide-angle correction for waveplate components," *Laser Focus World* **43**(3), 59-62 (2007).

[19] T. Radhakrishnan,"The dispersion, birefringence and optical activity of quartz," *Proc. Indian Acad. Sci. A* **29**, 260–265 (1947).
[20] W. Q. Zhang, "General ray-tracing formulas for crystal," *Appl. Opt.* **31**(34), 7328-7331 (1992).
[21] F. E. Veiras, L. I. Perez, and M. T. Garea, "Phase shift formulas in uniaxial media: an application to waveplates," *Appl. Opt.* **49**(15), 2769-2777 (2010).
[22] M. Avendano-Alejo and M. Rosete-Aguilar, "Optical path difference in a plane-parallel uniaxial plate," *J. Opt. Soc. Am. A* **23**(4), 926-932 (2006).
[23] M. Bass and V. N. Mahajan, [Handbook of Optics (3rd Edition), Volume I: Geometrical and Physical Optics, Polarized Light, Components and Instruments], McGraw-Hill, 13.2-13.5 (2010).
[24] H. G. Gu, C. W. Zhang, H. Jiang, X. G. Chen, W. Q. Li, and S. Y. Liu, "Measurement errors induced by axis tilt of biplates in dual-rotating compensator Mueller matrix ellipsometers," *Proc. SPIE* **9526**, 952617 (2015).
[25] P. J. M. van Laarhoven and E. H. L. Aarts, [Simulated annealing: theory and applications], Reidel, Dordrecht, (1988).